

Metal-free Carbon and Oxygen-doped Hexagonal Boron Nitride Photocatalysts for Degradation of Organic Pollutants

Feng Liu, Postgraduate student

Key Laboratory for Anisotropy and Texture of Materials (Ministry of Education), Northeastern University, Shenyang 110819, China, School of Civil & Environmental Engineering, University of Technology Sydney, Sydney, NSW 2007, Australia

Rui Han, Postgraduate student

Key Laboratory for Anisotropy and Texture of Materials (Ministry of Education), Northeastern University, Shenyang 110819, China, School of Civil & Environmental Engineering, University of Technology Sydney, Sydney, NSW 2007, Australia,

***Andrew Nattestad**, DECRA Research Fellow

ARC Centre of Excellence for Electromaterials Science, Intelligent Polymer Research Institute, Australian Institute for Innovative Materials, University of Wollongong, Wollongong, NSW 2525, Australia, anattestad@uow.edu.au (A. Nattestad), [0000-0002-1311-8951](tel:0000-0002-1311-8951)

***Xudong Sun**, Professor

State Key Laboratory of Rolling and Automation, Northeastern University, Shenyang 110819, China, xdsun@neu.edu.cn (X. Sun)

***Zhenguo Huang**, Associate Professor

School of Civil & Environmental Engineering, University of Technology Sydney, Sydney, NSW 2007, Australia, zhenguo.huang@uts.edu.au (Z. Huang), +61 2 95142661, [0000-0003-1985-0884](tel:0000-0003-1985-0884)

Carbon- and oxygen-doped hexagonal boron nitrides (BCNOs) with good chemical stability and photoresponsiveness to visible light are found to be promising metal-free catalysts for degradation of Rhodamine B. By doping with heteroatoms of carbon and oxygen, insulating h-BN was transformed into semiconducting BCNO. The BCNO photocatalyst presents photodegradation performance towards Rhodamine B (RhB), with degradation rates up to 1.39 hr⁻¹ (0.05 wt% catalyst loading). The active species involved in the photoreaction were demonstrated to be superoxide anion radical ([•]O₂⁻) and holes (h⁺), as opposed to [•]OH in the most studied TiO₂. The stability of BCNO in highly acidic environments was exploited for catalyst regeneration, as is necessary after long term use and poisoning. This work demonstrates that BCNO is a promising low-cost and metal-free photocatalyst for environmental pollution remediation.

Notation list

<i>CB</i>	conduction band
<i>VB</i>	valance band
<i>E_g</i>	bandgap of the semiconductor photocatalysts
<i>C_t</i>	absorbance of the solution after a certain time <i>t</i>
<i>C₀</i>	absorbance of the solution after a certain time <i>t</i>
<i>k</i>	photocatalytic rate constant
<i>t</i>	irradiation time
<i>h</i>	Planck's constant
<i>ν</i>	light frequency of the semiconductor photocatalysts

Research article

band structure, photocatalyst, degradation, etching, semi-conductors

1. Introduction

Non-metallic two-dimensional (2D) materials with unique electronic structures and good chemical stability have attracted strong research attention in the field of photochemistry.¹ These 2D materials, including graphene, graphitic carbon nitride (g-C₃N₄), black phosphorus (BP) and hexagonal boron nitride (h-BN) have shown promise in various photocatalytic applications such as hydrogen evolution by

water-splitting, CO₂ reduction and degradation of organic pollutants.²⁻⁶ h-BN is isostructural to graphene, but has a very different electronic structure compared to the gapless graphene.^{7,8} h-BN's chemical inertness and high thermal stability make it highly desirable in a number of applications.⁹⁻¹² Pristine h-BN's insulating nature and wide band gap (≈ 5.5 eV) exclude the excitation of electrons from the valence band to the conduction band under solar irradiation,^{13,14} and thus h-BN based materials are usually coupled with conventional semiconductors such as BiOBr,¹⁵ AgI/AgBr,^{16,17} TiO₂,^{18,19} and g-C₃N₄ in photocatalysis.^{20,21}

Recent theoretical calculations and experiments demonstrated the feasibility of transforming the insulating h-BN into a semiconductor by introducing carbon and oxygen heteroatoms.²²⁻²⁴ Due to the differences in electronegativity among B (2.0), C (2.5), N (3.0) and O (3.4), carbon and oxygen doping leads to asymmetrical charge distribution and formation of defects.^{7,25,26} By adjusting the carbon and oxygen contents in the h-BN network, the bandgap energy and optical properties of h-BN can be altered, making it suitable for sunlight-driven photocatalysis.^{27,28} Previously we reported versatile carbon- and oxygen- doped hexagonal boron nitride (BCNO) phosphors for anticounterfeit application,²⁸ where it was observed that emissions could be tuned by controlling carbon and oxygen contents. This study indicates the potential of BCNO to be applied in the photodegradation of organic pollutants. BCNOs demonstrate good chemical stability in acidic and alkaline conditions, which make them more suitable for harsh environments than many other commonly employed metal oxides, such as the widely studied BiVO₄ with limited stability in such pH conditions.²⁹ Catalyst poisoning is one of the main issues affecting the catalytic performance. Following extended use catalysts may become poisoned requiring regeneration. Thermal treatment is normally employed for this purpose, but this leads to a decrease in surface areas and is difficult to complete *in situ*.^{30,31} Acid or base washes are another approach to tackle this problem, but are only appropriate for materials with high chemical stability, such as BCNO. It is also noted that the photocatalytic nature of these materials may help limit soiling of the anticounterfeit structures.²⁸

In this study, BCNOs were used to degrade an organic pollutant photo-catalytically. A number of BCNOs were prepared through a facile pyrolysis method previously reported by our group.²⁸ The BCNO catalysts show high photocatalytic activities due to their reduced band gaps and strong visible light responsiveness. These low-cost, high-yield, and metal-free BCNOs also demonstrate high stability in acidic solutions which makes them promising for photocatalytic applications in harsh environments.

2. Experimental section

2.1 Synthesis of BN powders and BCNO photocatalyst

A detailed experimental protocol was previously reported,²⁸ so only key steps are listed here. Firstly, boric acid and melamine were dissolved in deionized water. After vigorous stirring, evaporation and vacuum drying, white powders were obtained and then heat treated at 1000 °C for 2h under Ar, leading to black BCN powders. These BCN samples were further heated at different temperatures (550, 650, 750 °C) with a fix dwell time (3h) in air. For samples treated at 850 °C, a shorter dwell time of 1h was used to prevent agglomeration and vitrification. The obtained colorful powders are denoted as BCNO-X, where X is the temperature, i.e. BCNO-550, BCNO-650, BCNO-750 and BCNO-850.

2.2 Materials characterization

X-ray diffraction (XRD) patterns were recorded on a D8 Bruker Discover with Cu K α ($\lambda = 1.54$ Å). Scanning electron microscopy (SEM) was conducted on a Zeiss Supra 55VP to observe the morphology of the powders. High-resolution imaging, energy dispersive X-ray spectroscopy (EDS) mapping, and electron energy loss spectroscopy (EELS) were carried out on a scanning transmission electron microscope (STEM) (JEOL ARM200F, operating at 80 kV). X-ray photoelectron spectroscopy (XPS) studies were performed on a PHOIBOS 100 hemispherical analyzer using Al K α (1486.6 eV) as the X-ray source. Fourier-transform infrared (FTIR) spectroscopy (Nicolet 6700 Spectrometer) was used to determine the chemical bonds. Raman spectra were obtained at room temperature using Renishaw Raman Spectroscopy with a laser source at 633 nm. Gas adsorption studies were carried out using a Quantachrome Autosorb MP instrument and surface areas were determined using Brunauer-Emmett-Teller (BET) calculations. The UV-visible absorption spectra were obtained using a Shimadzu UV-3600 spectrophotometer. Mott-Schottky plots were measured on a CHI 660E electrochemical workstation at the frequency of 1000 Hz in a standard three-electrode system. A Pt electrode and a Ag/AgCl (saturated KCl) electrode were used as a counter and reference, respectively. Zeta potential was measured by Malvern Zetasizer Nano-ZS.

2.2 Photocatalytic experiments

Photocatalytic activities of the synthesized BCNO powders were studied by degrading Rhodamine B (RhB in water, 20 mg L⁻¹) (Sigma-Aldrich) under simulated solar illumination (1 sun equivalent, 100 mW·cm⁻²). A 100 W Xenon lamp (Newport, LCS-100 Solar Simulators model 94011A) with an AM1.5 G filter was used as the light source. In a typical procedure, 10 mg catalyst was dispersed into

20 mL of the RhB solution. Prior to irradiation, the mixture was magnetically stirred overnight in the dark in order to attain an adsorption-desorption equilibrium. At irradiation time intervals of 10 min, 3 mL dye solution was collected, centrifuged to remove the photocatalyst particles and the concentration of RhB was measured using an UV-vis spectrophotometer (Agilent Technologies Cary 60 UV-Vis). After that, the collected solution and catalyst powders were returned to the reactor. 1 mM scavengers of isopropanol (IPA), p-benzoquinone (BQ, Sigma-Aldrich), triethanolamine (TEOA, Alfa Aesar) were used to investigate the mechanisms of dye degradation. For cycling tests, 50 mg of the catalysts were dispersed into 100 mL RhB (20 mg L⁻¹) solution to ensure enough material for post-reaction characterization. After each cycle, BCNO powders were collected through vacuum filtration with a PTFE membrane and then soaked in concentrated nitric acid (Sigma-Aldrich, ≥ 65%) for 15 minutes at room temperature. After acid wash, powders were washed repeatedly with distilled water and ethanol, and then added to a fresh RhB (20 mg L⁻¹) solution.

3. Results and discussion

3.1. Structural and morphological properties

BCN was prepared using a template-free method under Ar, and BCNO samples were then synthesized by annealing BCN under dry air at different temperatures. XRD patterns (Figure 1a) show two broad reflections centered at approximately 26.6° and 42.7° that are associated with (002) and (100) diffractions of h-BN.^{5,32} After heat treatment in air, the (002) reflection becomes stronger, implying an improved crystallinity. The chemical structure was further characterized using Raman and XPS. Owing to high level of carbon impurities in BCN and BCNO-550, a broad Raman peak (Figure S1) at around 1615 cm⁻¹ was observed. High temperature treatment removed most carbon and a broad peak appeared at around 1373 cm⁻¹ that is associated with E_{2g} vibration of BN.³³ Figure 1b-d show the XPS spectra of BCNO-750, where B-N, B-O and N-C components can be clearly seen in the deconvolutions. The presence of B-N components in both B1s and N1s indicates the formation of *sp*²-hybridized BN phase. Oxygen atoms bonded with boron are attributed to N₂-B-O (191.8 eV) and B-O (192.9 eV) structures, which originate from the substitution of oxygen atoms in the BN lattice and boric acid, respectively.^{22,34} In these structures, carbon atoms are primarily bound to nitrogen atoms, with residual N-H stemming from melamine used as a precursor.²⁸

SEM images (Figure 2a-d and S2) show that the samples have a rod-like morphology. After heat treatment in dry air, BCNO microrods became shorter in length and larger in diameters as compared to BCN (Figure 2a and S2a). A porous structure can be clearly seen in the BCNO-650 sample (Figure 2b and S2b), which probably originates from the escape of CO₂ due to the oxidation of carbon. For samples treated at higher temperatures such as BCNO-750 (Figure 2c and S2c) and BCNO-850 (Figure 2d and S2d), a greater number of rods with larger diameters and shorter lengths are observed, which is likely caused by sintering. The high-resolution TEM (HRTEM) imaging shows that lattice fringes become more clearly defined (Figure 2e and S3) as the temperature increases, indicating better crystallinity. XPS (Figure 1b), EELS spectrum (Figure 2f) and EDS mapping (Figure 2g) results confirm that BCNOs consist of four elements, namely B, C, N, and O. EDS mapping reveals a uniform distribution of these elements throughout the selected area, confirming the uniform doping of carbon and oxygen in BCNO. EELS spectrum exhibits four characteristic B, C, N and O K-edge peaks with discernible π^* and σ^* peaks, proving that B, C, N and O are in a *sp*²-hybridized structure.^{28,32} XPS results on other BCNO samples reveal similar chemical compositions.²⁸

3.2. Optical properties and energy band structures

Through XPS and EELS techniques, carbon and oxygen were confirmed existed in BN matrix. The doping level of C and O in h-BN can be effectively modulated by controlling heat treatment temperatures, which in turn tunes the optoelectrical properties of h-BN. The optical properties of BCNO were measured by diffuse reflectance spectroscopy (DRS).²⁸ The most intense absorption features were seen at shorter wavelengths around 400 nm, with notable shoulders (and in the case of BCNO-850 a distinct second peak) at around 830 nm. Tauc plots were used to evaluate bandgaps (Figure 3a) and the band gap energies (E_g) were determined to be 2.25 eV, 2.50 eV and 2.85 eV for BCNO-650, BCNO-750 and BCNO-850, respectively. All BCNO samples possess a narrower band gap than pristine h-BN (\approx 5.5 eV), indicating enhanced light harvesting properties. The blue shift of the absorption peaks of BCNO, as well as the long absorption tail, result from reduced surface defects and the presence of carbon quantum dots and surface states, respectively. These discussed in greater detail in our previous report.²⁸

Figure 3b shows the Mott-Schottky plots of BCNO samples with positive fitting lines, indicating n-type nature of BCNO. The conduction band (CB) edge potentials for BCNO-650, BCNO-750 and BCNO-850 are determined to be -1.09, -0.92 and -0.85 V (vs. AgCl/Ag, pH=7) based on the measured electrochemical flat-band potentials,^{34,35} which can be converted to -0.893, -0.723, -0.653 V (vs. NHE,

pH=7).³⁶ Based on this and the optical band gaps discussed above, band energy structures of BCNO are presented in Figure 3c. The valence band (VB) edge potentials of BCNO-650, BCNO-750 and BCNO 850 are 1.357, 1.777 and 2.197 V (vs. NHE, pH=7), respectively.

3.3. Photocatalytic activity measurements

To evaluate photocatalytic performance of BCNO, Rhodamine B (RhB) was first selected as a model pollutant. Prior to the photodegradation process, the catalyst was added to the dye solution and stirred overnight in the dark in order to attain an adsorption-desorption equilibrium. The Zeta potentials (Figure S4) were measured to be around -33 mV for all samples in ultrapure water, indicating the negative charged state of BCNO samples. By inspecting the adsorption/desorption equilibrium of RhB after overnight stirring, BCNO-750 exhibits highest adsorption capacity among BCNO samples (BCNO-750 > BCNO-650 > BCNO-850 > BCNO-550) (see Figure S5). It can be seen that the adsorption performance depends on the surface area of samples. Nitrogen sorption experiments (Figure S6) indicate that all the BCNO samples have low specific surface areas, in the range of 4.2-11.5 m²/g, of which BCNO-750 possesses the highest value. Table S1 shows that BCNO-750 has the lowest RhB packing density, in the order of BCNO-850 > BCNO-650 > BCNO-750. Photocatalytic activity of BCNO samples were evaluated by degrading RhB under simulated solar light, with the photodegradation rates evaluated by the first order equation:

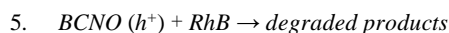
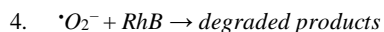
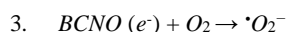
$$1. \quad kt = -\ln(C_t / C_0)$$

where k is the photocatalytic rate constant, C₀ the initial concentration of RhB solutions, and C_t is the concentration of RhB solution after time t.

Figure 4a and S7 show that the photocatalytic activity of BCNO samples depends strongly on the treatment temperature, increasing from 0.102 hr⁻¹ for 550 °C to 1.39 hr⁻¹ for 750 °C. RhB without a catalyst was seen to be quite stable during the 80-minute period of irradiation used here. The sample processed at 850 °C provides a lower photocatalytic activity (1.166 hr⁻¹) as compared to BCNO-750, but still much higher than BCNO-550. The differences in photocatalytic activity are believed to be associated with the combination of light harvesting and the chemical driving forces for radical generation. The smaller band gap, resulting from carbon and oxygen doping, is beneficial to broaden the absorption range of visible light, leading to enhancement of photodegradation activity under simulated sunlight. As such, the temperature of heat treatment affects the photocatalytic performance through the variation in composition and structure. Higher temperature (750 and 850 °C) treatment reduces the amount of free carbon and leads to carbon and oxygen structural doping, as evidenced by XPS and EELS. Low temperature treatment such as 550 °C fails to remove large amount of carbon and to introduce sufficient oxygen doping. The optical properties of BCNO-550 are thus notably different from the other BCNO samples, without distinct absorption peaks and having an extended tail.²⁸ At the other end of the examined range, high temperature processing (850 °C) reduces carbon doping and increases oxygen doping, leading to a large band gap and decreased light harvesting efficiency. Besides the optical properties, treatment temperature also affects the surface area, an important factor for photocatalytic activity which occurs at the interface. With increased processing temperature, the surface area of BCNO samples actually increased, which is assumed to result from the formation of CO₂ due to oxidization of carbon, supported by SEM images in Figure 2. On the other hand, treatment at 850 °C led to short and wide rods in morphology, and lower surface areas (Figure S6), resulting in less RhB adsorption as well as lower photodegradation rate. The higher RhB packing density of BCNO-850 may also limit access of active radicals or O₂ to the surface. Additionally, the higher CB potential of BCNO-850 compared to BCNO-750 indicates that the driving force might be a bit low for BCNO-850 to generate superoxide effectively (further discussion on the mechanism is presented below). It can then be concluded that 750 °C represents the optimal processing temperature to control the composition and band energy structure of BCNO for this application. The degradation of RhB over BCNO-750, monitored by absorption spectroscopy, is shown in Figure S8. Each experiment was repeated three times and average values taken, along with calculations of the standard deviation as an error.

An indirect chemical probe method was employed to investigate the mechanisms of photodegradation of RhB over the BCNO samples. It is known that organic bonds are attacked by active species such as holes (h⁺), hydroxyl radicals (•OH) and superoxide anion radicals (•O₂⁻) in photocatalytic oxidation processes.^{37,38} In order to get a clear understanding of the mechanism, scavengers of IPA, BQ and TEOA were introduced into the photoreaction to quench •OH, •O₂⁻ and h⁺ active species, respectively. The photocatalytic degradation performance of BCNO-750 and BCNO-850, with the additions of the above-mentioned quenchers were investigated under simulated solar irradiation (Figure 4b and S9). BCNO-750 and BCNO-850 show similar results with the addition of BQ almost completely quenching dye degradation, which indicates •O₂⁻ to be the primary active species in these systems. Additionally, some suppression was observed upon the addition of TEOA, implying that h⁺ is also active in BCNO photocatalysis systems. According to band energy analysis,

the CB edge potentials (-0.723 V and -0.653 V vs NHE) of BCNO-750 and BCNO-850 are both more negative than the standard redox potential of O_2/O_2^- (-0.33 V vs NHE), suggesting that electrons in the CB of BCNO can reduce O_2 .³⁹ However, the oxidation potential of $\cdot OH/OH^-$ (+2.40 V) is more positive than VB of BCNO-750 and BCNO-850 (+1.777 V and +2.197 V vs NHE, respectively), indicating that holes at the VB edge cannot easily oxidize H_2O to $\cdot OH$.⁴⁰ Under simulated solar illumination, photoexcited electrons in the CB of BCNO can reduce O_2 to form superoxide anion radicals ($\cdot O_2^-$), while the corresponding holes in the VB of BCNO can directly react with RhB.^{21,34,41} The possible pathways of photocatalytic reactions could be described as followings:



In contrast, the degradation rates remain almost unchanged in the presence of IPA, suggesting a limited role played by $\cdot OH$. $\cdot OH$ is the primary active species for many photocatalysts such as TiO_2 , but it can be quenched by even small quantities of some alcohols.³⁸ The insensitivity of our system suggests that BCNO could find applications in waste streams where alcohols, or other quenchers of $\cdot OH$ radicals are present. On the basis of band edge analysis and experimental results, the possible mechanism for photodegrading RhB is depicted in Figure 4c.

During long-term operation, it is expected that contamination and poisoning of the catalysts will occur. The conventional method to regenerate catalysts is by oxidative treatment in air.^{31,42} This may, however, lead to compositional changes, for example, the loss of boron due to formation of boron oxide.²⁸ As such, a different approach was used in this work, which is using nitric acid to remove tightly adsorbed organic residue. It was found that the photodegradation performance of BCNO-750 after washing was nearly the same as the first run (Figure 5). Figure S10-12 show the stability of BCNO-750 after repeated washing in nitric acid, displaying no discernible changes in morphology (Figure S10), chemical structure (Figure S11), and crystal structure (Figure S12), respectively. In addition, we found that BCNOs are also stable in basic environment such as 30% NH_3 aqueous solution.²⁸ The high thermal stability and chemical stability allow for broader applications of BCNOs in various environments than some other photocatalysts such as $BiVO_4$ that is unstable in acidic solution.^{29,43} The photocatalytic degradation of methylene blue over BCNOs was also tested. After certain periods of simulated solar illumination, the concentration of methylene blue decreased significantly. Further testing on other common organic pollutants are also underway.

4. Conclusion

In summary, BCNO photocatalysts synthesized via facile pyrolysis show effective photodegradation of Rhodamine B. Heat treatment temperature plays a key role in modulating the doping levels of C and O in BCNOs, in turn the optoelectronic structure. BCNO-750, with a bandgap of 2.5 eV, shows the highest photocatalytic activity and maintains its performance after being washed using strong nitric acid, indicating potential applications in certain harsh environment. Different from the commonly used TiO_2 , the main active species in photodegradation were identified as $\cdot O_2^-$ and h^+ , indicating its suitability for applications in alcohol-containing solutions. The inexpensive starting materials, facile synthetic methods, controllable optoelectronic properties and high photodegradation performance, all make BCNO a promising metal-free photocatalyst. Further processing to increase surface area will improve the likelihood of photoexcited charges in BCNO reaching interfaces where they can generate radicals and increase the number of organic molecules tethered in proximity to said radicals. Consequently, this is expected to lead to enhanced degradation performance.

Acknowledgments

This research was funded partially by the Australian Government through the Australian Research Council (ARC) (project number DP170101773). Z.H. is the recipient of an ARC Future Fellowship (project number FT190100658). A.N. appreciates the support by the ARC Centre of Excellence for Electromaterials Science and ARC Discovery Early Career Researcher Award (DE160100504).

References

1. Luo B, Liu G and Wang L (2016) Recent advances in 2D materials for photocatalysis. *Nanoscale* **8**(13): 6904-6920.
2. Zhang H, Lv X, Li Y, Wang Y and Li J (2009) P25-graphene composite as a high performance photocatalyst. *ACS Nano* **4**(1): 380-386.
3. Wang X, Maeda K, Thomas A, Takanabe K, Xin G, Carlsson JM, Domen K and Antonietti M (2009) A metal-free polymeric photocatalyst for hydrogen production from water under visible light. *Nature Materials* **8**(1): 76.
4. Liu D, Zhang M, Xie W, Sun L, Chen Y and Lei W (2017) Porous BN/TiO₂ hybrid nanosheets as highly efficient visible-light-driven photocatalysts. *Applied Catalysis B: Environmental* **207**: 72-78.
5. Shankar R, Sachs M, Francàs L, Lubert-Perquel D, Kerherve G, Regoutz A and Petit C (2019) Porous boron nitride for combined CO₂ capture and photoreduction. *Journal of Materials Chemistry A* **7**(41): 23931-23940.
6. Zhu M, Kim S, Mao L, Fujitsuka M, Zhang J, Wang X and Majima T (2017) Metal-free photocatalyst for H₂ evolution in visible to near-infrared region: black phosphorus/graphitic carbon nitride. *Journal of the American Chemical Society* **139**(37): 13234-13242.
7. Fan M, Wu J, Yuan J, Deng L, Zhong N, He L, Cui J, Wang Z, Behera SK and Zhang C (2019) Doping Nanoscale Graphene Domains Improves Magnetism in Hexagonal Boron Nitride. *Advanced Materials* **31**(12): 1805778.
8. Han R, Liu F, Wang X, Huang M, Li W, Yamauchi Y, Sun X and Huang Z (2020) Functionalised hexagonal boron nitride for energy conversion and storage. *Journal of Materials Chemistry A* **8**(29): 14384-14399.
9. Han R, Khan MH, Angeloski A, Casillas G, Yoon CW, Sun X and Huang Z (2019) Hexagonal Boron Nitride Nanosheets Grown via Chemical Vapor Deposition for Silver Protection. *ACS Applied Nano Materials* **2**(5): 2830-2835.
10. Khan MH, Liu HK, Sun X, Yamauchi Y, Bando Y, Golberg D and Huang Z (2017) Few-atomic-layered hexagonal boron nitride: CVD growth, characterization, and applications. *Materials Today* **20**(10): 611-628.
11. Khan MH, Jamali SS, Lyalin A, Molino PJ, Jiang L, Liu HK, Taketsugu T and Huang Z (2017) Atomically thin hexagonal boron nitride nanofilm for Cu protection: the importance of film perfection. *Advanced Materials* **29**(4): 1603937.
12. Xiao F, Naficy S, Casillas G, Khan MH, Katkus T, Jiang L, Liu H, Li H and Huang Z (2015) Edge -hydroxylated boron nitride nanosheets as an effective additive to improve the thermal response of hydrogels. *Advanced Materials* **27**(44): 7196-7203.
13. Kubota Y, Watanabe K, Tsuda O and Taniguchi T (2007) Deep ultraviolet light-emitting hexagonal boron nitride synthesized at atmospheric pressure. *Science* **317**(5840): 932-934.
14. Guo Y, Wang R, Wang P, Rao L and Wang C (2018) Dredged-Sediment-Promoted Synthesis of Boron-Nitride-Based Floating Photocatalyst with Photodegradation of Neutral Red under Ultraviolet-Light Irradiation. *ACS Applied Materials & Interfaces* **10**(5): 4640-4651.
15. Di J, Xia J, Ji M, Wang B, Yin S, Zhang Q, Chen Z and Li H (2016) Advanced photocatalytic performance of graphene-like BN modified BiOBr flower-like materials for the removal of pollutants and mechanism insight. *Applied Catalysis B: Environmental* **183**: 254-262.
16. Wu W, Lv X, Wang J and Xie J (2017) Integrating AgI/AgBr biphasic heterostructures encased by few layer h-BN with enhanced catalytic activity and stability. *Journal of Colloid and Interface Science* **496**: 434-445.
17. Zhou C, Lai C, Zhang C, Zeng G, Huang D, Cheng M, Hu L, Xiong W, Chen M and Wang J (2018) Semiconductor/boron nitride composites: synthesis, properties, and photocatalysis applications. *Applied Catalysis B: Environmental* **238**: 6-18.
18. He Z, Kim C, Jeon TH and Choi W (2018) Hydrogenated heterojunction of boron nitride and titania enables the photocatalytic generation of H₂ in the absence of noble metal catalysts. *Applied Catalysis B: Environmental* **237**: 772-782.
19. Wang N, Yang G, Wang H, Yan C, Sun R and Wong C-P (2019) A universal method for large-yield and high-concentration exfoliation of two-dimensional hexagonal boron nitride nanosheets. *Materials Today* **27**: 33-42.
20. Yang Y, Zhang C, Huang D, Zeng G, Huang J, Lai C, Zhou C, Wang W, Guo H and Xue W (2019) Boron nitride quantum dots decorated ultrathin porous g-C₃N₄: intensified exciton dissociation and charge transfer for promoting visible-light-driven molecular oxygen activation. *Applied Catalysis B: Environmental* **245**: 87-99.
21. Jiang L, Yuan X, Zeng G, Wu Z, Liang J, Chen X, Leng L, Wang H and Wang H (2018) Metal-free efficient photocatalyst for stable visible-light photocatalytic degradation of refractory pollutant. *Applied Catalysis B: Environmental* **221**: 715-725.
22. Weng Q, Kvashnin DG, Wang X, Cretu O, Yang Y, Zhou M, Zhang C, Tang DM, Sorokin PB and Bando Y (2017) Tuning of the optical, electronic, and magnetic properties of boron nitride nanosheets with oxygen

- doping and functionalization. *Advanced Materials* **29(28)**: 1700695.
23. Lu Q, Zhao Q, Yang T, Zhai C, Wang D and Zhang M (2018) Preparation of boron nitride nanoparticles with oxygen doping and a study of their room-temperature ferromagnetism. *ACS Applied Materials & Interfaces* **10(15)**: 12947-12953.
 24. Huang C, Chen C, Zhang M, Lin L, Ye X, Lin S, Antonietti M and Wang X (2015) Carbon-doped BN nanosheets for metal-free photoredox catalysis. *Nature Communications* **6**: 7698.
 25. Zhang X, Li L, Lu Z, Lin J, Xu X, Ma Y, Yang X, Meng F, Zhao J and Tang C (2014) Effects of carbon and oxygen impurities on luminescence properties of BCNO phosphor. *Journal of the American Ceramic Society* **97(1)**: 246-250.
 26. Liu L, Sham T-K and Han W (2013) Investigation on the electronic structure of BN nanosheets synthesized via carbon-substitution reaction: the arrangement of B, N, C and O atoms. *Physical Chemistry Chemical Physics* **15(18)**: 6929-6934.
 27. Sivaprakash K, Induja M and Priya PG (2018) Facile synthesis of metal free non-toxic Boron Carbon Nitride nanosheets with strong photocatalytic behavior for degradation of industrial dyes. *Materials Research Bulletin* **100**: 313-321.
 28. Liu F, Nattestad A, Naficy S, Han R, Casillas G, Angeloski A, Sun X and Huang Z (2019) Fluorescent Carbon - and Oxygen - Doped Hexagonal Boron Nitride Powders as Printing Ink for Anticounterfeit Applications. *Advanced Optical Materials* **7(24)**: 1901380.
 29. Kim TW and Choi K-S (2016) Improving stability and photoelectrochemical performance of BiVO₄ photoanodes in basic media by adding a ZnFe₂O₄ layer. *The journal of physical chemistry letters* **7(3)**: 447-451.
 30. Saoud WA, Assadi AA, Guiza M, Bouzaza A, Aboussaoud W, Ouederni A, Soutrel I, Wolbert D and Rtimi S (2017) Study of synergetic effect, catalytic poisoning and regeneration using dielectric barrier discharge and photocatalysis in a continuous reactor: Abatement of pollutants in air mixture system. *Applied Catalysis B: Environmental* **213**: 53-61.
 31. Argyle MD and Bartholomew CH (2015) Heterogeneous catalyst deactivation and regeneration: a review. *Catalysts* **5(1)**: 145-269.
 32. Zhang H-W, Li Y-Y, Huang W-Q, Zhou B-X, Ma S-F, Lu Y-X, Pan A-L and Huang G-F (2019) Hollow BCN microrods with hierarchical multichannel structure as a multifunctional material: Synergistic effects of structural topology and composition. *Carbon* **148**: 231-240.
 33. Xiao F, Chen Z, Casillas G, Richardson C, Li H and Huang Z (2016) Controllable synthesis of few-layered and hierarchically porous boron nitride nanosheets. *Chemical Communications* **52(20)**: 3911-3914.
 34. Feng C, Tang L, Deng Y, Zeng G, Wang J, Liu Y, Chen Z, Yu J and Wang J (2019) Enhancing optical absorption and charge transfer: Synthesis of S-doped h-BN with tunable band structures for metal-free visible-light-driven photocatalysis. *Applied Catalysis B: Environmental*, doi: <https://doi.org/10.1016/j.apcatb.2019.117827>: 117827.
 35. Liu Q, Chen C, Du M, Wu Y, Ren C, Ding K, Song M and Huang C (2018) Porous hexagonal boron nitride sheets: effect of hydroxyl and secondary amino groups on photocatalytic hydrogen evolution. *ACS Applied Nano Materials* **1(9)**: 4566-4575.
 36. Gao X, Feng J, Su D, Ma Y, Wang G, Ma H and Zhang J (2019) In-situ exfoliation of porous carbon nitride nanosheets for enhanced hydrogen evolution. *Nano Energy* **59**: 598-609.
 37. Zhu J-N, Zhu X-Q, Cheng F-F, Li P, Wang F, Xiao Y-W and Xiong W-W (2019) Preparing copper doped carbon nitride from melamine templated crystalline copper chloride for Fenton-like catalysis. *Applied Catalysis B: Environmental*, doi: <https://doi.org/10.1016/j.apcatb.2019.117830>: 117830.
 38. Pingmuang K, Chen J, Kangwansupamonkon W, Wallace GG, Phanichphant S and Nattestad A (2017) Composite photocatalysts containing BiVO₄ for degradation of cationic dyes. *Scientific reports* **7(1)**: 8929.
 39. Trang TNQ, Phan TB, Nam ND and Thu VTH (2020) In situ charge transfer at the Ag@ ZnO photoelectrochemical interface toward the high photocatalytic performance of H₂ evolution and RhB degradation. *ACS Applied Materials & Interfaces* **12(10)**: 12195-12206.
 40. Li B, Lai C, Zeng G, Qin L, Yi H, Huang D, Zhou C, Liu X, Cheng M and Xu P (2018) Facile hydrothermal synthesis of Z-scheme Bi₂Fe₄O₉/Bi₂WO₆ heterojunction photocatalyst with enhanced visible light photocatalytic activity. *ACS Applied Materials & Interfaces* **10(22)**: 18824-18836.
 41. Tian L, Li J, Liang F, Chang S, Zhang H, Zhang M and Zhang S (2019) Facile molten salt synthesis of atomically thin boron nitride nanosheets and their co-catalytic effect on the performance of carbon nitride photocatalyst. *Journal of Colloid and Interface Science* **536**: 664-672.
 42. Lei W, Portehault D, Liu D, Qin S and Chen Y (2013) Porous boron nitride nanosheets for effective water cleaning. *Nature Communications* **4**: 1777.
 43. Pingmuang K, Nattestad A, Kangwansupamonkon W, Wallace GG, Phanichphant S and Chen J (2015) Phase-controlled microwave synthesis of pure monoclinic BiVO₄ nanoparticles for photocatalytic dye degradation. *Applied Materials Today* **1(2)**: 67-73.

Figure caption list:

Figure 1. a) XRD pattern; b) XPS survey scan, XPS spectra of c) B1s and d) N1s of BCNO-750

Figure 2. SEM images of a) BCN; b) BCNO-650; c) BCNO-750; d) BCNO-850. Scale bars are 400 nm. HRTEM image of e) BCNO-750; f) EELS spectrum of BCNO-750; EDS mapping of g) BCNO-550

Figure 3. a) Tauc plots of BCNO samples. b) Mott-Schottky plots measured in 0.5M Na₂SO₄ (vs. Ag/AgCl). c) Schematic energy band diagram, with reported redox potentials for radical generation

Figure 4. a) Photodegradation rates for RhB over BCNOs; b) Photodegradation rates for RhB over BCNO-750 and BCNO-850 with and without scavengers; c) Schematics of proposed degradation mechanism

Figure 5. Photodegradation of Rhodamine B over the BCNO-750 before and after washing using concentrated nitric acid
